Food Hydrocolloids 58 (2016) 98–112

Contents lists available at ScienceDirect

Food Hydrocolloids

journal homepage: www.elsevier.com/locate/foodhyd

Molecular interactions, characterization and photoactivity of Chlorophyll *a*/chitosan/2-HP-β-cyclodextrin composite films as functional and active surfaces for ROS production

Vito Rizzi [a], Paola Fini [b], Fiorenza Fanelli [c], Tiziana Placido [a], Paola Semeraro [a], Teresa Sibillano [d], Aurore Fraix [e], Salvatore Sortino [e], Angela Agostiano [a, b], Cinzia Giannini [d], Pinalysa Cosma [a, b, *]

[a] *Università degli Studi di Bari "Aldo Moro", Dipartimento di Chimica, Via Orabona, 4, I-70126 Bari, Italy*
[b] *Consiglio Nazionale delle Ricerche CNR-IPCF, UOS Bari, Via Orabona, 4, 70126 Bari, Italy*
[c] *Consiglio Nazionale delle Ricerche CNR-NANOTEC, Via Orabona, 4, 70126 Bari, Italy*
[d] *Consiglio Nazionale delle Ricerche CNR-IC, Via Amendola 122/O, 70126 Bari, Italy*
[e] *Laboratory of Photochemistry, Department of Drug Sciences, University of Catania, Viale Andrea Doria 6, I-95125 Catania, Italy*

ARTICLE INFO

Article history:
Received 4 November 2015
Received in revised form
8 February 2016
Accepted 11 February 2016
Available online 18 February 2016

Keywords:
Chitosan films
Chlorophyll *a*
Active packaging
Singlet oxygen
Cyclodextrins

ABSTRACT

Novel photosensitizing film based on the natural hybrid polymer Chitosan/2-hydroxy-propyl-β-Cyclodextrin (CH/CD) is synthesized introducing Chlorophyll *a* (CH/CD/Chl*a*) as a photoactive agent for possible application in antimicrobial photodynamic therapy (PDT). The polymer absorbs visible light, in turn able to generate reactive oxygen species (ROS) and, therefore it can be used as environmental friendly and biodegradable polymeric photosensitizer (PS). The modified film is characterized by means of different spectroscopic, calorimetric, diffraction techniques and microscopic imaging methods including time-resolved absorption spectroscopy. UV–Vis, FTIR-ATR and X-ray Photoelectron Spectroscopy (XPS) analyses suggest that Chl*a* shows a strong affinity toward Chitosan introducing interactions with amino groups present on the polymer chains. Nanosecond laser flash photolysis technique provides evidence for the population of the excited triplet state of Chl*a*. Photogeneration of singlet oxygen is demonstrated by both direct detection by using infrared luminescence spectroscopy and chemical methods based on the use of suitable traps. Scanning Electron Microscopy (SEM), Atomic Force Microscopy (AFM) and Differential Scanning Calorimetry (DSC) analyses confirm also the occurrence of structural changes both on the film surface and within the film layer induced by the insertion of the pigment. Moreover, X-ray Diffraction data (XRD) shows the existence of an amorphous phase for the chitosan films in all the compared conditions.

1. Introduction

Since several years, the problem involving the emergence of antibiotic resistance among pathogenic bacteria (Hamblin & Hasan, 2004; Yoshikawa, 2002), seems to lead to the end. Indeed, in several institutions around the world a more effective alternative for antibacterial treatments have been developed (Cerveny, De Paola, Duckworth, & Gulig, 2002; Sajjan et al., 2001; Wainwright, 1998). Among them, Photodynamic Therapy (PDT), *i.e.* the combination of a light source with a photosensitizing agent (PS) and endogenous molecular oxygen is considered as a practical therapy for these diseases (Fu, Jordan, & Samson, 2013; Rizzi et al., 2014a). In fact, the rapid growth and mutations of bacteria, able to facilitate microbes surviving in the presence of an antibiotic drug, will quickly become predominant throughout the microbial population. Additionally, since the indiscriminate and inappropriate use of antibiotics, the problem get worse (Yoshikawa, 2002). Interestingly, for recent years PDT has appeared useful for treatments of several problems as for example those related to food safety, in which a significant number of man-made activities could induce the contamination of food products (Balali, Grelier, Benaissa & Coma,

* Corresponding author. Università degli Studi di Bari "Aldo Moro", Dipartimento di Chimica, Via Orabona, 4, I-70126 Bari, Italy.
E-mail address: pinalysa.cosma@uniba.it (P. Cosma).

http://dx.doi.org/10.1016/j.foodhyd.2016.02.012
0268-005X/

2008). As a consequence, the concept of Active Packaging becomes an interesting alternative to the traditional use of the conventional package, *i.e*. a passive barrier protecting the food. In European Community such new innovative concept has been defined as "a type of packaging that changes the condition of the packaging to extend shelf-life or improve safety or sensory properties while maintaining the quality of the food" (Gomez-Estaca, Lopez-de-Dicastillo, Hernandez-Munoz, Catala, & Gavara, 2014; Vermeiren, Devlieghere, Van Beest, De Kruijf, & Debevere, 1999). In general, active food packaging provides additional functions that do not exist in conventional packaging systems and not only protect food passively and physically against environmental agents, but also inhibits or retards bacteria growth. Among different active packaging approaches (Gomez-Estaca et al., 2014; Vermeiren et al., 1999), the incorporation of active substances to the packaging material is an attractive development. Not surprisingly, the quality of packaged foods can be improved by controlling the release of these active agents reducing the growth rate of dangerous microorganisms or inactivating it by contact (Quintavalla & Vicini, 2002). On the other hand, due to the decrease of fossil resources, the food packaging materials based on natural macromolecules from renewable resources have received great attention (Coma, 2013; Pedersen, Stæhr Wernberg, &Thomsen, 2005). In fact, in recent years and in different fields, the main attention has been focused on the Biomass, occurring to be a renewable energy source (Coma, 2013; Pedersen, Stæhr, Wernberg, & Thomsen, 2005). In such context, the attention of this paper has been focused on Chitosan (CH) as inexpensive, biodegradable, biocompatible, nontoxic and environmentally friendly linear amino polysaccharide derived from chitin, a major component of insects and crustacean shells. CH was chosen among biopolymers for the high-quality film forming properties and antimicrobial activity (Bordenave, Grelier, Pichavant, & Coma, 2005; Bordenave, Grelier, & Coma, 2010) useful for several applications (Moczek & Nowakowska, 2007; Rabea, Badawy, Stevens, Smagghe, & Steurbaut, 2003). CH contains more than 5000 glucosamine units and it is obtained commercially from shrimp and crab shell chitin (a N-acetylglucosamine polymer) by alkaline deacetylation. For several years, bioactive CH matrices have been used in food preservation (Davies, Elson, & Hayes, 1989; El Ghaouth, Arul, Grenier, & Asselin, 1992; El Ghaouth, Arul, Ponnampalam, & Boulet, 1991; Jiang & Li, 2001; Muzzarelli & Rocchetti, 1986; Rabea et al., 2003). More specifically, in recent years, the CH chemical modification by inserting photoactive groups acting as potential PS for application in photosensitized oxidation reactions in water has been developed (Moczek & Nowakowska, 2007).

The pioneering works of Krausz *and co-workers* (Mbakidi et al., 2013), and related references, highlight the interest in this field of research, also in the recent past. For example, Krouit *and co-workers* (Krouit, Granet, Branland, Verneuil, Krausz, 2006) showed their new photoantimicrobial films composed of porphyrinated lipophilic cellulose esters and also the photobactericidal films from porphyrins grafted to alkylated cellulose (Krouit, Granet, Krausz, 2009).

Many kind of applications can be listed, however among them it is worth mentioning the work of Ringot *and co-workers* (Ringot et al., 2011) highlighting that porphyrins maintain their properties as PSs when grafted to polysaccharides, *i.e*. chitosan or cellulose, obtaining modified polymers as photobactericidal membranes or films for various applications.

Starting from results obtained by Krausz, and thanks to our experience on a natural chlorine, Chl*a*, solubilized in different systems (Agostiano, Catucci, Cosma, & Fini, 2003; Agostiano, Cosma, Trotta, Monsù-Scolaro, & Micali, 2002; Dentuto et al., 2007), the development of CH film containing such pigment, for potential application as bioactive antimicrobial packaging material, is presented for the first time in this paper as a novel photoactive system. Nonetheless the excellent CH properties, the system Chl*a*/CH presents several limitations due to the acid pH condition necessary for the preparation of CH hydrogel. In fact, CH is insoluble in water, but soluble in dilute organic acids which induce the protonation of CH free amino groups (Rabea et al., 2003), with pH condition not suitable for the chemical stability of Chl*a*. Hence the standard procedure used in literature to prepare CH films from hydrogel was modified in order to optimize the condition for introducing Chl*a*.

It is ascertained in literature that CH films (indicated in the text as CH STD) were generally prepared by the method described by B. Krajewska (Krajewska, Leszko, & Zaborska, 1990; Krajewska, 1991) in which a 1% (v/v) solution of CH is dissolved in 0.8% (v/v) aqueous acetic acid solution. The acidity of the medium is too high and induces the chemical degradation of Chl*a* with the release of the central Mg atom, inducing the loss of the chemical properties of the pigment. In our proposed procedure the pH of CH hydrogel is maintained at about 6 units, value at which Chl*a* is chemically stable. 2-HP-β-CD (or CD) has been used to promote chitosan polymer chains association (Burns et al., 2015). As for the photodynamic properties of PS-modified CH film, recent literature has shown that PSs conjugated with CH chains (Shrestha & Kishen, 2012) or saccharide like-structures (Cellamare, Fini, Agostiano, Sortino, & Cosma, 2013) retained their photoactive properties making it a possible option for PDT applications. On the other hand, only one paper by P. Mandal and co-workers (Mandal, Manna, Das, & Mitra, 2015), was known in literature related to Chl*a* molecules and chitosan hydrogel as scaffold, for application in artificial light harvesting antenna. In this paper, stacked Chl*a* molecules were entrapped within the chitosan matrix, then the pigment is not in its monomeric form and it is not photoactive (Mandal et al., 2015).

Starting from these considerations a comprehensive investigation on the CH/CD/Chl*a* film properties has been thus undertaken in our laboratories using several complementary techniques, namely spectroscopic, calorimetric, X-ray diffraction analyses and microscope imaging methods. A comparison of Chitosan biofilms arisen from our innovative procedure (with and without CD) with those well characterized in literature and arisen from a well-known procedure have been also performed in order to strengthens similarity and differences between them. In addition, for the first time, in order to show the photoactivity of the hybrid system CH/Chl*a*, among ROS, Singlet Oxygen is searched for. Nanosecond laser flash photolysis technique provides evidence for the population of the excited triplet state of Chl*a* and the photogeneration of singlet oxygen is demonstrated by both direct detection by using infrared luminescence spectroscopy and chemical methods based on the use of suitable traps. The main results arising from such characterization involving Chl*a* in solid state device will be described in the present paper opening new horizons in an enhanced antimicrobial activity of chitosan film for possible applications in PDT.

2. Experimental Section

2.1. Materials

All the chemicals used were of analytical grade and samples were prepared using double-distilled water. Commercial grade Chitosan powder (CH, from crab shells, with a molecular weight of 150,000, highly viscous, with a hypothetical deacetylation degree $\geq$ 75%), Acetic acid (99,9%), EtOH (99,9%) and glycerol (99,9%) were purchased from Sigma Aldrich.

The deacetylation degree has been experimentally estimated. Among several methods proposed for measuring the real degree of

acetylation, DS(Ac), of CH, ^{1}H NMR (700 MHz) and FTIR-ATR analyses have been used.

As for this purpose, Equations (1) and (2) have been used for NMR and IR obtained data, respectively (Kasaai, 2008; Baxter, Dillon, Taylor, & Roberts, 1992; Lavertu et al., 2003). Chitosan powder (1% v/v) was dissolved in D_2O and deuterated acetic acid (0.8% v/v) medium for NMR analysis and trimethylsilyl-propionic-2,2,3,3-d4 acid, (TSP), has been used as a references. Conversely, for FTIR-ATR ones, CH STD solid state film was directly analysed.

$$DS(Ac)\% = \left(1 - \left(\frac{1}{3}H_{Ac} \Big/ \frac{1}{6}H_{26}\right)\right) \times 100 \quad (1)$$

$$DS(Ac)\% = \left[100 - \left(\frac{A_{1637}}{A_{3450}}\right) \times 115\right] \quad (2)$$

H_{Ac} (δ2.50 ppm) and H_{26} (δ4.20 ppm) represent the calculated experimental integrals of the indicated protons and, A_{1637} and A_{3450} represent the intensity of the IR signals at indicated wavenumbers (see FTIR-ATR section for the assignment of the vibration modes) also corrected with baselines proposed in literature (Baxter et al., 1992).

Not surprisingly, NMR and IR results were agreed between them, giving a DS(Ac) % around 30% confirming the manufacturer's Sigma Aldrich specification. Chl*a* was extracted and purified from spinach leaves using Omata and Murata method (Omata & Murata, 1980) whose details can be found in Supplementary Material.

Chl*a* stock solutions were stored in acetone at −80 °C. 2-HP-β-CD was purchased from Fluka and used without further purification.

2.2. Procedure for CH film preparation

We propose the same procedure recently applied by some Authors of this paper (Rizzi et al., 2014b). CH powder was dissolved in 0.1% (v/v) aqueous acetic acid solution, in order to obtain a 2% (w/v) of Chitosan, by constant continuous stirring for 24 h to obtain an homogeneous solution. 200 μL of glycerol were added every 100 mL of CH acetic solution. Then, the solution was filtered through a coarse sintered glass filter due to the great amount of CH not dissolved and degassed for 1 h. The reduced acetic acid amount and the excess of CH ensures the neutral pH occurring to be 6 unit. After degassing, the CH solution was poured into a plastic Petri plate. The latter was maintained in an oven at 60 °C for 24 h. A thin (CH) membrane was obtained. The same procedure was followed to obtain (CH/CD) films modified with 2-HP-β-CD used as a cross-linker. In particular, the 2-HP-β-CD powder was added to chitosan hydrogel obtaining a solution having a final concentration of 10^{-3} M.

The difficulty of incorporating water insoluble Chl*a* molecules in CH/CD films has been circumvented by means of the casting technique from EtOH solution: 2 × 2 cm squared pieces of CH/CD free standing films were soaked with an EtOH solution containing Chl*a* (10^{-3} M) at 25 °C for 24 h resulting in a successful entrapment of the pigment inside the as prepared films. The outer surface of CH/CD/Chl*a*-modified films were washed with double-distilled water and air-dried before performing any characterization. All samples have been analysed at least in triplicate. The amount of Chl *a* loaded inside the CH/CD film was 0.12 ± 0.02 g/cm^2, obtained evaluating the difference between the amount of Chl*a*, presents in EtOH solution, before and after the adsorption on CH/CD film.

2.3. X-ray Photoelectron Spectroscopy (XPS) analysis

XPS analyses were performed using a Thermo Electron Theta Probe spectrometer equipped with a monochromatic Al Ka X-ray source (1486.6 eV) operated at a spot size of 300 μm corresponding to a power of 70 W. Survey (0–1400 eV) and high resolution (C1s, O1s, N1s and Mg1s) spectra were recorded in FAT (fixed analyzer transmission) mode at pass energy of 200 and 100 eV, respectively. All spectra were acquired at a take-off angle of 37° with respect to the sample surface. Charge compensation was accomplished by a low energy electron flood gun (1 eV). Special care was devoted during the analysis to verify that no change in the samples was induced by exposure to the X-ray beam and the electron flood gun. XPS analysis was repeated on three different spots for each sample. Charge correction of the spectra was performed by taking the hydrocarbon (C–C, C–H) component of the C1s spectrum as internal reference (binding energy, BE = 285.0 eV). Atomic percentages were calculated from the high resolution spectra using the Scofield sensitivity factors set in the ThermoAvantage V4.87 software (Thermo Fisher Corporation) and a non-linear Shirley background subtraction algorithm. The best-fitting of the high-resolution XPS spectra was performed using with mixed Gaussian–Lorentzian peaks after a Shirley background subtraction; a maximum relative standard deviation of 10% was estimated on the area percentages of the curve-fitting components, while the determined standard deviation in their position was ±0.2 eV.

2.4. Differential Scanning Calorimetry (DSC)

DSC measurements were performed with a Q200 TA Instruments thermal analyzer calibrated with indium as standard.

For thermogram acquisition, sample sizes of 1–2 mg were scanned with a heating rate of 5 °C/min over a temperature range from 25 °C to 300 °C. Dry material was placed in an aluminum cup and hermetically sealed. Chl*a* samples were prepared by casting from ethanol solution in the aluminum caps. Empty cup was used as a reference and runs were performed in triplicate. Samples were analyzed under continuous flux of dry nitrogen gas (50 mL/min).

2.5. UV–Visible and FTIR-ATR spectroscopic measurements

UV–Vis absorption spectra were recorded using a Varian CARY 5 UV–Vis-NIR spectrophotometer (Varian Inc., now Agilent Technologies Inc., Santa Clara, CA, USA). FTIR-ATR spectra were recorded within the 600–4000 cm^{-1} range using an Fourier Transform Infrared spectrometer 670-IR (Varian Inc., now Agilent Technologies Inc., Santa Clara, CA, USA), whose resolution was set to 4 cm^{-1}. 32 scans were summed for each acquisition.

2.6. Water Vapor Transmission Rate (WVTR)

WVTR of CH based materials was evaluated using 7002 Water Vapor Permeation Analyzer (Illinois Instruments, Inc. U.S.). The instrument displays the WVTR as either g/m^2/day or g/100in2/day and into the instrument is incorporated a Pb_2O_5 sensor. According to the Faraday's Combined Laws of Electrolysis, the electrolytic current is a measure of the rate at which water is electrolyzed. Under equilibrium conditions this equals the rate at which moisture is being absorbed by the Pb_2O_5 film. Thus, knowledge of the gas flow rate through the housing and the current in the cell gives an absolute measure of the moisture contained in the sample gas. The films were stored in the cell at 25 ± 1 °C and 90 ± 1% relative humidity (RH) for 24 h.

2.7. Scanning Electron Microscopy (SEM)

The surface morphology of the CH, CH/CD and CH/CD/Chl*a* films was investigated using a Zeiss SUPRA™ 40 field emission scanning electron microscope (FE-SEM). SEM images were acquired with a

conventional Everhart-Thornley detector at the working distance of 5 mm and electron acceleration voltage of 0.6 kV.

2.8. Atomic Force Microscopy (AFM)

AFM experiments were performed by a PSIA XE-100 SPM system in AFM mode, and cantilevers with silicon nitride tips were used. Topography images were recorded in non-contact mode at a 1 Hz scan rate with a resolution of 512 × 512 pixels.

2.9. X-ray diffraction (XRD)

X-ray diffraction data were collected at room temperature from CH standard, CH, CH/CD, CH/CD/Chl*a* and CH/CD in EtOH films Measurements were performed at a fixed incident angle of 3° by a Bruker D8 Discover diffractometer, equipped with a Göbel mirror, using Cu Kα radiation ($\lambda_{K\alpha1} = 1.54056$ Å and $\lambda_{K\alpha2} = 1.54439$ Å), and a scintillation detector. The working conditions were set to 40 kV and 50 mA. Data were collected in the range 5–60° with a step size of 0.1°.

2.10. Laser flash photolysis setup

The sample was excited with the third harmonic of a Nd–YAG Continuum Surelite II–10 laser (355 nm, 6 ns, ~10 mJ). The quartz plate with the chitosan-based film was aligned at an angle of 45° with respect to both the excitation and the monitoring beams. The reflection of the excitation from the quartz plate was to the opposite side of the transient signal detection. The measurements in solution were carried out with a 10 × 10 mm^2 quartz cell with a 3 mL capacity. The excited sample was analyzed with a Luzchem Research mLFP–111 apparatus with an orthogonal pump/probe configuration. The probe source was a ceramic xenon lamp coupled to quartz fiber-optical cables. The laser pulse and the mLFP–111 system were synchronized by a Tektronix TDS 3032 digitizer, operating in pre-trigger mode. The signals from a compact Hamamatsu photomultiplier were initially captured by the digitizer and then transferred to a personal computer, controlled by Luzchem Research software operating in the National Instruments LabView 5.1 environment. The sample temperature was 295 ± 2 K. The energy of the laser pulse was measured at each shot with a SPHD25 Scientech pyroelectric meter.

2.11. Direct detection of $^1O_2$

Steady-state emission of $^1O_2$ in the NIR region was recorded with a Fluorolog-2 Mod-111 spectrometer, equipped with a InGaAs detector maintained at −196 °C, by illuminating the film sample, immersed in a quartz cuvette filled D_2O and placed at 45° with respect the excitation beam, with a 405 nm CW laser (2 W cm^{-2}).

2.12. Photoactivity measurements

In order to demonstrate the photoactivity of chitosan film containing Chl*a*, direct and indirect methods were employed to achieve our aim. 4-thiothymidine (S^4TdR, Carbosynth Limited, UK) and Singlet Oxygen Sensor Green (SOSG, Molecular Probes, Inc. by Life Technologies Limited, Scotland) have been used in aqueous solution at concentration of 10^{-5} M and 1.5 μM, respectively. These aqueous solutions containing a slice film 1 × 1 cm were illuminated with a neon lamp, whose emission had been previously assessed to occur mainly between 400 and 700 nm and with a power surface density of 60 mW/cm^2. The solution absorption or emission spectra were recorded at different times of irradiation. S^4TdR absorption spectra were recorded in the range of 200–800 nm ($\lambda^{max} = 337$ nm in aqueous solution and 326 in D_2O). SOSG emission was registered at 525 nm ($\lambda_{ex} = 488$ nm). Its maximum absorption peak was at about 500 nm. Chitosan film containing-Chl*a* absorption spectra were recorded in the range of 350–800 nm.

As far as SOSG, it is reported in literature (Cellamare et al., 2013) as a highly selective singlet oxygen fluorescent probe with a fluorescein moiety bound to an anthracene derivative. The reaction with singlet oxygen increases the observed emission at 525 nm due to the generation of an endoperoxide specie as a main product. A 550 nm cut-off glass filter has been used to reduce the self-production of $^1O_2$ by SOSG. Measurements were achieved before irradiation and every 10 min for 100 min. As far as S^4TdR is concerned, it is a modified nucleoside able to react with singlet oxygen without, at moment, selectivity in the presence of ROS. Moreover our recent studies show its high photostability, if solution was irradiated with visible light (Rizzi et al., 2014a). Measurements were achieved before irradiation and after 100 min.

As far as the irradiation of Chitosan film-containing Chl*a*, it has been realized, directly, with a slice film (1 × 1 cm) putted on neon lamp, and UV–Visible absorption-measurements have been performed before irradiation and every 10 min for 100 min employing a supporting film-device. The fluorescence measurements were conducted using a spectrofluorimeter Varian CARY Eclipse 68. A quartz cuvette with an optical path length of 1 cm has been employed for all spectroscopic measurements.

3. Results and discussion

3.1. UV–Vis spectroscopy analysis

As already known (Ryan & Senge, 2015), the molecular structure of Chl*a* shows typical features: the heteroaromatic character of the porphyrin system, the central metal and a long chain made of carbon atoms (Ryan & Senge, 2015). As a preliminary study based on UV–Vis spectroscopy, the spectrum (350–800 nm) of polysaccharide film, CH/CD, containing Chl*a* (CH/CD/Chl*a*), entrapped by soaking in an ethanolic solution, was acquired and reported in Fig. 1a. The camera picture of a large sample CH/CD/Chl*a* is reported in Fig. 1 showing the homogeneous distribution of Chl*a* inside the film. At first glance, a characteristic Chl*a* absorption spectrum is clearly observed. The spectrum is characterized by an intense Soret band at about 422 nm, in the blue region of the visible spectrum, and a $Q_Y(0,0)$ band, in the red region, at about 663 nm (Manna, Basu, Mitra & Mukherjee, Das, 2009; Omata & Murata, 1980). In accordance with our experience and by comparing the spectrum showed in Fig. 1a with one recorded in alcoholic solution and reported in Fig. 1b, (in which the Chl*a* occurs in its monomeric and photoactive form), it is evident that inside the CH/CD film (Fig. 1a) the pigment maintains its active form (Agostiano et al., 2003, 2002a; Dentuto et al., 2007). Interestingly, a detailed observation of the absorption spectrum reveals a significant ipsochromic shift of the Soret band (from 430 nm in alcoholic solution to 419 nm in CH/CD film), which appears unstructured, broadened and also characterized by a hyperchromic effect. In addition, a slight blue shift of the $Q_Y(0,0)$ band was revealed if compared with the same band recorded in the ethanolic solution (Fig. 1b). It is worth mentioning that the spectral differences can be better observed by means of the first derivative analysis of the UV–Vis absorption spectrum of the CH/CD/Chl*a* film (Fig. 1a, inset). The Soret band indicates the presence of two spectral components located at 403 and 430 nm, respectively. More specifically, the two latter correspond to different conformations and orientations of the Chl*a* porphyrin macrocycle inside the film.

These results suggest that different interactions between Chl*a* and CH/CD-composite film were established, involving a change in

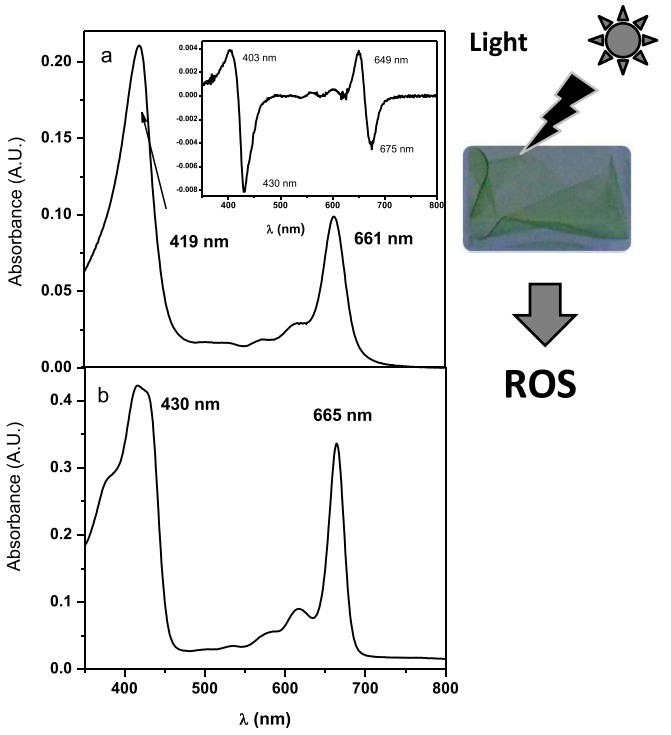

Fig. 1. UV–Visible Absorption spectra of (a) CH/CD film containing Chla and (b) Ethanolic solution of Chla at concentration of 10^{-5} M. Inset 1a: First derivative analysis of UV–Vis absorption spectrum of CH/CD film containing Chla. The camera picture of a large sample CH/CD/Chla showing the homogeneous distribution of Chla inside the film.

chitosan chains coordination due to the symmetry of Chl*a*-porphyrin ring in chitosan film (Mandal et al., 2015).

Accordingly, also the first derivative analysis performed on the absorption band located at 661 nm shows the presence of two spectral components ascribable to different forms of the pigment: (i) a monomer form and (ii) a hydrated dimeric one (Agostiano et al., 2003, 2002a; Dentuto et al., 2007) represented by signals located at 649 nm and at 675 nm, respectively (Agostiano, Catucci, Colafemmina & Scheer, 2002). Comparable wavelength values were also reported in literature, for Chl*a* solubilized in aqueous surfactants solutions and in water–organic solvent mixtures (Agostiano et al., 2002a, b; Agostiano, Cosma, Della Monica, & Fong, 1990; Agostiano, Catucci, Colafemmina, & Della Monica, 1996; Agostiano, Cosma, & Della Monica, 1991; Agostiano et al., 2002), proving our considerations. More specifically, the interaction of Chl*a* with positive charges, able to induce a blue shift of the Q_Y band together with the lack of resolution of the Soret band at 419 nm (Agostiano, Catucci, Colafemmina, & Scheer, 2002b) was suggested. Additionally, such observed broadening, at 419 nm, can be related to strong interactions between Chl*a* and Chitosan chains (Mandal et al., 2015). In conclusion the spectral components located at 675/430 nm indicate the interactions between CH/CD and Chl*a* *via* water molecules (Mandal et al., 2015; Agostiano et al., 2002b, 1990, 1996, 1991, 2002a; Chauvet, Viovy, Santus& Land, 1981), while those located at 403/649 nm suggest the interactions with positive charged (Mandal et al., 2015; Ryan & Senge, 2015; Agostiano et al., 2002b) amino groups present on CH chains.

In order to draw more detailed information on the interactions leading to the generation of CH/CD/Chl*a* blended film, and to gain insights into the surface chemical composition of the blended films prepared in this work, XPS analyses were carried out on the CH film produced with the new procedure after immersion in ethanol, the CH/CD film after immersion in EtOH and the CH/CD/Chl*a* film.

In order to evidence only similarities and differences between CH STD and CH or CH/CD, and thus to show the property of the latter, from now and when it was necessary for a question of clarity, the results related to CH STD have been reported every time.

3.2. XPS analysis

XPS atomic percentages are reported in Table S2, while the high-resolution XPS C1s and N1s spectra and the summary of the curve-fitting results are shown in Fig. 2 and Table 1, respectively.

The C1s spectrum of the CH film, prepared by means of our novel procedure (Fig. 2a), is curve fitted with four peaks (Beamson & Briggs, 1992; Roy, Samanta, Mukherjee, Roy, & Mukherjee, 2013; Kang, Liu, Zheng, Qu, & Chen, 2010): the hydrocarbon component at 285.0 eV (C1, 30%) due to adventitious hydrocarbon contamination and to a possible contribution of methyl groups of acetate anions, the most abundant component at 286.5 eV (C2, 56%) ascribed to both C–N and C–O groups present in the chitosane polymer, the peak at 288.1 (C3, 13%) assigned to both N–C=O groups in N-acetylglucosamine units and O–C–O moieties, the very weak peak at 289.1 eV (C4, 1%) due to carboxylate groups of acetate anions. The N1s spectrum is composed by a principal component at 399.7 eV, ascribed to both unprotonated amino and amide groups (N2, 93%), and a second weak component at 401.5 eV associated to protonated amino groups (N3, 7%) (Roy et al., 2013; Kang et al., 2010).

No significant variations are observed in the XPS C1s and N1s signals when 2-HP-β-CD is present in the film (Fig. 2b), in fact, comparable curve-fitting results are obtained for CH and CH/CD films. On the other hand, the presence of Chl*a* in the CH/CD/Chl*a* film induces a remarkable variation of the XPS C1s signal (Fig. 2c); in particular the considerable increase of the peak area percentage of the hydrocarbon component at 285.0 eV can be ascribed to Chl*a* and, specifically, to contributions from the phytyl chain, aromatic carbon atoms of the porphyrinic ring, alkyl and alkenyl substituents of the porphyrinic ring. Noticeably the N1s spectrum of the CH/CD/Chl*a* film shows a new component at 398.3 eV attributed to nitrogen atoms in the Chl*a* porphyrin macrocycle (Brace et al., 1978; Karweik & Winograd, 1976; Bekalé, Barazzouk, & Hotchandani, 2012a; Bekalé, Barazzouk, & Hotchandani, 2012b). Interestingly, the ratio between the peak area percentages of the N3 (NH_3^+) and N2 (NH_2/N–C=O) components increases from 0.075, as observed for both CH and CH/CD films (N2 and N3 peak percentages of 93% and 7%, respectively), to about 0.12 in the case of the CH/CD/Chl*a* film (N2 and N3 peak percentages of 78% and 9%, respectively); this confirm, in excellent agreement with the so far discussed hypothesis, a rearrangement of the CH chains induced by Chl*a* incorporation suggesting a novel disposition of the protonated amino groups on the film surface arising from novel coordination as well suggested by Mandal et al. (2015).

3.3. Differential Scanning Calorimetry

Additional information on CH, CH/CD and CH/CD/Chl*a* films was searched for through DSC analysis. It was ascertained in literature that polysaccharides show strong affinity for water and in the solid state a disordered structures that can be easily hydrated has been already proposed (Harish Prashanth, Kittur, & Tharanathan, 2002; Pereira Jr., Queiroz de Arruda & Stefani, 2015). Indeed, calorimetric studies on analogue systems indicate a weight loss, from polymer, in four consecutive steps. The first two steps (endothermic) are due to the loss of surface water from biofilm; the third and fourth ones (exothermic) are due to the decomposition process (Pereira, Queiroz de Arruda, & Stefani, 2015) of the acetylated and deacetylated units of the polymer and its cracking (Pereira et al.,

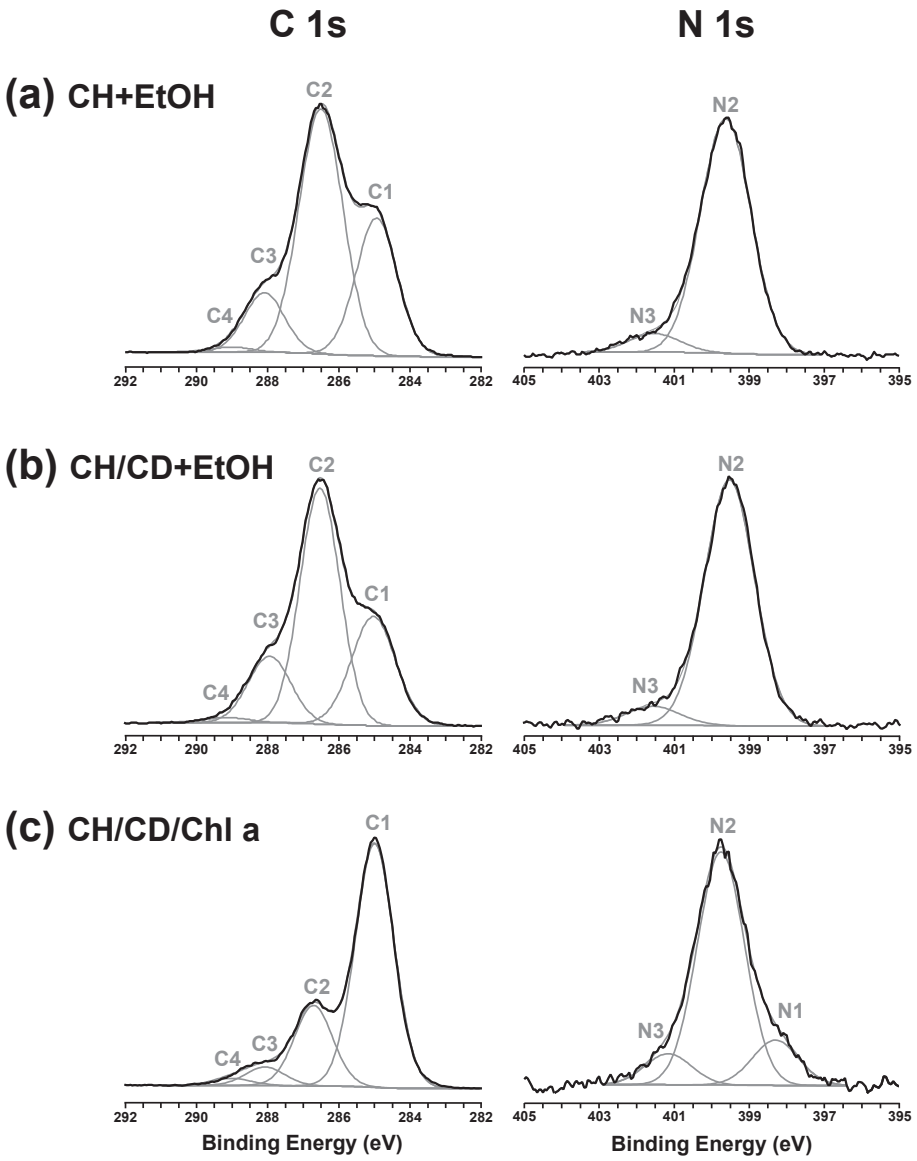

Fig. 2. High-resolution XPS C 1s and N 1s spectra of (a) the CH film prepared with the new method (CH) after immersion in ethanol, (b) the CH/CD film after immersion in ethanol and (c) the CH/CD/Chla film.

Table 1
Curve-fitting results of the high-resolution XPS C 1s and N 1s spectra of (a) the CH film prepared with the new method after immersion in ethanol, (b) CH/CD film after immersion in ethanol and (c) CH/CD/Chl a film.

Signal	Component	Binding energy [eV]	Assignments	Relative peak area [%]		
				(a) CH + EtOH	(b) CH/CD + EtOH	(c) CH/CD/Chl *a*
C1s	C1	285.0	C–C, C–H, C=C	30	29	68
	C2	286.5	C–O, C–N	56	54	24
	C3	288.1	O–C–O, C=O,N–C=O	13	16	6
	C4	289.1	O–C=O	1	1	2
N 1s	N1	398.3	=N–			13
	N2	399.7	NH_2, N–C=O	93	93	78
	N3	401.5	NH_3^+	7	7	9

2015; Kittur, Harish Prashanth, Sankar, & Tharanathan, 2002).

The main DSC curves related to CH, CH/CD and CH/CD/Chl*a* films are showed in Fig. 3 and a comparison has been undertaken also with Chl*a* samples prepared by casting from ethanol solution in the aluminum caps (Fig. 3a).

CH film thermogram, in agreement with what reported in literature (Pereira et al., 2015; Kittur et al., 2002) for the well-known CH STD, displays an endothermic phase (from 40 °C to 150 °C), due to the evaporation of water, and an exothermic phase (in the range 240°C–300 °C) due to Chitosan degradation (Fig. 3b).

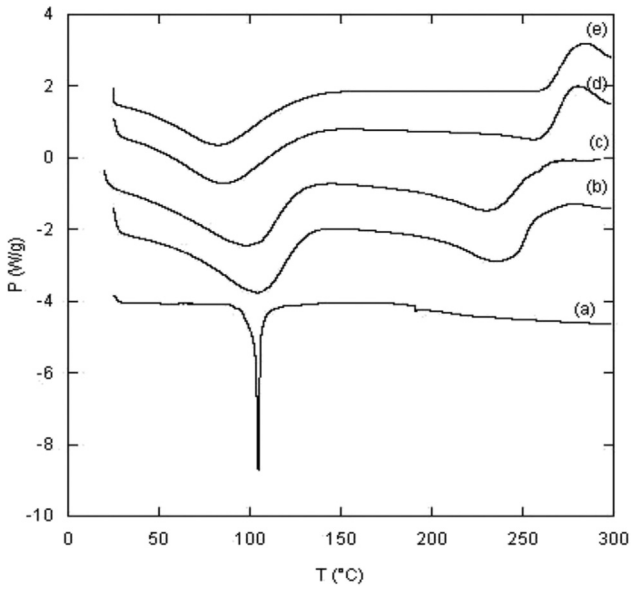

Fig. 3. Comparison between detailed views (Temperature range: 0–300 °C) of DSC thermograms of (a) Chla samples prepared by casting from ethanol solution in the aluminum caps and different composite films: (b) Chitosan films (CH); (c) Chitosan films (CH) containing 2-HP-β-CD (CH/CD); (d) CH/CD treated with EtOH; (e) CH/CD containing Chla (CH/CD/CHla).

Interestingly, looking all thermograms, differences in the endothermic peak areas and positions have been observed indicating different water–polymer interactions (Harish Prashanth et al., 2002).

More specifically, the presence of CD in CH films produces a slight shift of the first broad endothermic peak associated to the loss of water towards lower temperature and a decrease in its area (Fig. 3c). In other words CH film containing CD shows lower hydrophilic character likely due to a different organization of polymeric chains. The less amount of water in the latter indicates a weaker interaction of water with films, leading a lower evaporation temperature. Not surprisingly, in accordance with Prashanth and co-workers (Harish Prashanth et al., 2002) the presence of CD does not induce any important changes in the peak associated to the degradation process (Karweik & Winograd, 1976). As for the EtOH effect on CH/CD film, the thermogram (Fig. 3d) reveals that such film occurs with more pronounced hydrophobic properties than the same previous the treatment (Fig. 3c). This is also confirmed by the clear lower amount of withheld water induced by the alcoholic dehydrating action. Additionally, the film occurs to be more stable than the CH and CH/CD ones.

On the other hand the incorporation of Chl*a* in CH/CD films (Fig. 3e) produces an opposite effect on the endothermic and exothermic peaks, associated respectively to water loss and film decomposition. The first one is shifted to lower temperature whereas the second one is moved towards higher temperature values. Thus the pigment makes films less hydrophilic and more stable than CH and CH/CD ones.

In addition, in the thermogram of CH/CD/Chl*a* film the melting peak of Chl*a* is not visible (Fig. 3a and e). It could be due to the presence, in the same temperature range, of the broad endothermic peak associated to the loss of water and/or to an absence of the melting pigment peak which should indicate that the pigment in such condition is present in an amorphous state.

In conclusion the further observed decrease in film affinity towards water due to presence of Chl*a* in CH/CD films was in agreement with those expected considering the hydrophobic character of the Chl*a* molecule. Differently, the increased film stability (film composition temperature occurs higher than 250 °C) is noteworthy since Chl*a* is not stable at such temperature. Thus, the presence of Chl*a* induces a reorganization of polymeric chains in the films affecting the thermal degradation process and as already explained in literature (Pereira Jr. et al., 2015; Kittur et al., 2002) such effect can be attributed to variation induced on amino group of chitosan chains. Results once again suggest the main role of Chitosan amino groups in Chl*a* and CH/CD film interactions.

3.4. FTIR-ATR spectroscopy measurements

In order to better understand the molecular organization of Chl*a* inside the CH/CD composite film, and thus detailing previous showed measurements, FTIR-ATR analyses were performed on CH film arising from the known standard procedure, CH film prepared with the new method, CH/CD and, last but not least, on CH/CD/Chl*a* films. Although similar to each other as a whole, FTIR spectra show slight differences in the absorption intensities and peak positions.

For the sake of comparison, in Fig. 4d, the FTIR spectra of CH STD (black line) and CH films (grey line) are reported, showing analogies and differences between the two different typologies of films. Thanks to previous studies related to chitosan films, it is possible to individuate the characteristic IR bands of CH in our condition: in the 3300–3400 cm^{-1} range (N–H, 3276 cm^{-1}, and O–H, 3346 cm^{-1}, stretching), the doublet (2923/2875 cm^{-1}) relative to the symmetric and asymmetric C–H stretching in the 2700–3000 cm^{-1} range, the amide I band (-NHR–CO– stretching) at 1637 cm^{-1} and at 1550 cm^{-1} there is the overlapping of the signal relative to the NH_2 bending (amide II) of chitosan with the carboxylate stretching vibrations of acetate anions, which presents also a signal at 1410 cm^{-1}. Bands occurring at 1151 cm^{-1} and 1059 cm^{-1} due to the C–O–C asymmetric and symmetric stretching, respectively, and at 1031 cm^{-1} due to the C–O stretching of the alcoholic moieties, are known to be typical for saccharide structure (Synytsya, Grafova, Slepicka, Gedeon, & Synytsya, 2012; El-Hefian, Nasef, & Yahaya, 2012; Liu, Adhikari, Guo, & Adhikari, 2013).

In general, for all spectra reported in Fig. 4 it is evident the absence of narrow absorption bands around 3300 cm^{-1} indicating the absence of free OH groups, conversely the occurrence, as expected, of intra and intermolecular hydrogen bonds were proposed in such condition in accordance with similar studies reported in literature (Burns et al., 2015). The region above 3000 cm^{-1} presents slight differences in the O–H and N–H band position and a shift to higher wavenumbers, from 3346/3276 cm^{-1} in the standard CH film to 3353/3294 cm^{-1} in the CH film containing Chl*a* and 2-HP-β-CD (Fig. 4a, d), indicating an increase of more ordered structures (Thakhienw, Devahastin&Soponronnarit, 2013 and reference therein). By comparing the two IR spectra referred to CH film prepared in accordance with standard (Fig. 4d, black line) and new method (Fig. 4d, grey line), at a first glance it is possible to observe that the neutral CH film presents the amide I band (carbonyl band) and the amide II band (bending of the aminic group) shifted to higher wavenumbers (the first one shifts from 1637 cm^{-1} to 1653 cm^{-1}, the second one from 1550 cm^{-1} to 1560 cm^{-1}). Moreover, the intensity ratio between the two bands appears reversed if the neutralized film (CH film) is considered. It is well known that these signals, as well the hydrogen bonding formation, are sensitive to the chitosan acetylation degree (DS(Ac)) and to the organic acid used for film preparation (El-Hefian et al., 2012; Liu et al., 2013; Thakhienw, Devahastin, & Soponronnarit, 2013; Nunthanid, Puttipipatkhachorn, Yamamoto, & Peck, 2001; Chen et al. 2011).

In particular the intensity of amide I signal decreases as a function of the DS(Ac), disappearing in completely deacetylated chitosan (Kasaai, 2008), whereas the amide II band shifts to higher

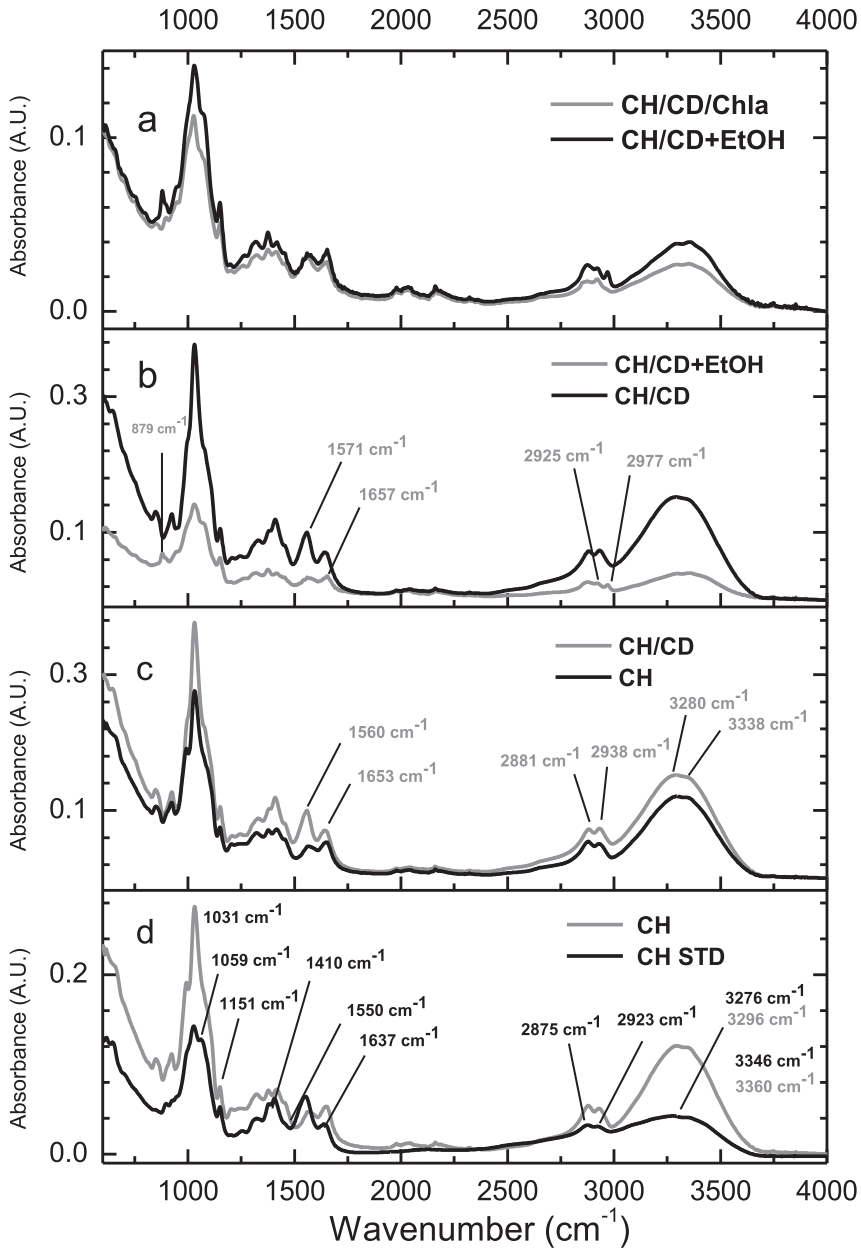

Fig. 4. Comparison between detailed views (wavenumber range: 600–4000 cm^{-1}) of ATR-FTIR spectra of different composite films: (a) Chitosan films (CH) containing 2-HP-β-CD in presence (gray line) and in absence (black line) of Chla; (b) Chitosan films containing 2HP-β-CD (CH/CD) before (black line) and after treatment with EtOH (gray line); (c) Chitosan films in presence (gray line, CH/CD) and in absence (black line, CH) of cyclodextrin; (d) Chitosan films obtained in accordance with standard procedure (black line CH STD) and chitosan film in accordance with our method (gray line, CH).

wavenumbers (Harish Prashanth et al., 2002). In our case the standard CH film spectrum (black line), which contains a greater amount of acetic acid (see Experimental Section), reveals that the signal relative to the protonated aminic group $-NH_3^+$ and generally present as a shoulder at about 1514 cm^{-1}, is completely absent (Demarger-Andre & Domard, 1994). This indicates that the acetic acid carboxylates interact ionically with positively charged amino groups on the CH chain reducing the amount of free amino groups as if the DS(Ac) of CH is lowered (Chen et al., 2008). Thus the inversion of the intensity ratio in the neutralized film is indicative of a reduced amount of acetate anion, which is unable to act as electrostatic cross-linker between the chitosan chains making less intense the mediated interchain interactions. This hypothesis is also confirmed by the narrowing and intensity increasing of the O–H and N–H stretching band and by the shift of the related wavenumbers indicative of a greater mobility (Burns et al., 2015). The addition of 2-HP-β-CD (Fig. 4c, gray line) to CH film essentially induces changes in the band positions which shift slightly to lower wavenumbers as a whole. In fact in general CD and chitosan are characterized by similar FTIR signals, but as 2-HP-β-CD amount is lower than CH one, the effect of the CD presence is evidenced by slight changes of the wavenumbers of CH spectral bands. Interestingly, in presence of CD, due to the great amount of O–H groups, the O–H and N–H stretching band, if compared with the same one without CD (see Fig. 4c, black line), occur broadened and slightly shifted at lower wavenumber indicating the involvement of both inter- and intramolecular hydrogen bonds between CH chains and cyclodextrin ones (Chen et al., 2008; Bostan et al., 2014). These

results are not surprising, in fact it was well known that CDs addition promotes chitosan polymer chains association (Burns et al., 2015). The C–H symmetric and asymmetric stretching (CH STD) shifts to higher wavenumbers: from 2923 to 2938 cm^{-1} and from 2875 to 2881 cm^{-1}, respectively. In particular these displacements could be also indicative of non-polar intermolecular interactions between CD and CH chains (Harish Prashanth et al., 2002). Amide I (1653 cm^{-1}) and the $-NH_2$ (1560 cm^{-1}) signals are very intense with the ratio again inverted. Furthermore, it is present a signal at 1410 cm^{-1} indicative of the presence in the CD-modified CH film of a greater amount of acetate anion as regards of the neutralized film without 2-HP-β-CD. This could be attributed to a greater difficulty in the acetic acid removal from the film due to the presence of cyclodextrin. This interaction between acetic acid/CD and CH is confirmed also by the bands in the region characteristic of glucopyranose (1100–900 cm^{-1}) which appear more intense and broader indicating non-polar interaction between CH chains and cyclodextrin ring (Wang et al., 2007). In general in the case of salts involving aminic groups the presence of strong hydrogen bonds determines an increase of the intensity and a broadening of the IR N–H signals together with a frequency lowering (Jug, Maestrelli, & Mura, 2012). For the CH film containing CD this situation is due to the 2-HP-β-CD ability of forming hydrogen bonds which increments the CH interchain distance allowing a higher penetration of the acetate anion which in turn interacts electrostatically with CH as shown by the absence of the signal relative to the $-NH_3^+$ group at about 1514 cm^{-1}.

Since the insertion of Chl*a* in the film has been obtained by dipping the CH film in an ethanolic solution containing the pigment, it has been evaluated the effect of the immersion of the film in ethanol. In Fig. 4b the comparison between the CH film with CD before and after the immersion in ethanol was showed. Clearly the contact with EtOH generates a novel disposition of CH chains, shielding them from detection (Burns et al., 2015) which results in a reduced absorption intensity of the film as a whole. This could be indicative of the presence of strong interactions due to additional interchain hydrogen bonds that partially block vibrational modes (Coates, 2000). This result is similar to the one obtained for CH STD (Fig. 4d), in which strong inter and intra chain interactions were established. Further signals appear at 2925 $cm^{-1}$and at 879 cm^{-1} ascribable to the EtOH presence in the film inducing chitosan chains rearrangement (Jug et al., 2012; He, Ao, Gong, & Zhang, 2011). In particular the ethanolic C–H stretching signal is localized at 2977 cm^{-1} and it predominates over the C–H stretching signal of the CH/CD system. This indicates that the film treatment with EtOH, dehydrating agent, determines the removal of the acetate anion, in accordance with literature (Coates, 2000), and residual water with the insertion of ethanol molecule in the formation of more extended hydrogen bonds, compacting the film. These added inter-chain interactions make more rigid the film vibrational mode (Coates, 2000 and reference therein). This is also confirmed by changes in the CH amide and amine signals in the region 1500–2000 cm^{-1}. More specifically, amide I signal shifts to 1657 cm^{-1}, while the aminic band shifts to 1571 cm^{-1} inverting their ratio. Moreover the acetate anion signal at 1410 cm^{-1} disappears.

The addition of Chl*a* in the CH/CD film does not evidence new bands or substantial modification in the position of film characteristic signals (Fig. 4a). The absence of the typical Chl*a* vibrational modes can be due, as expected, to the excess of chitosan and especially to the strong interactions between chitosan chains and Chl*a* restricting the vibrational mode of the latter (Mandal et al., 2015). On the other hand, it is possible to observe slight variations essentially due to disappearing of ethanol signals which determines a general intensity decrease of FTIR spectrum. The disappearance of the ethanolic signals induces a structural rearrangement of the film which results in a more compact structure. In fact in the range 2700–3000 cm^{-1}, typical of the C–H stretching, it is observed an inversion in the peaks intensity (Fig. 4a, gray line). Further, the signals in the 1200–1500 cm^{-1} range, typical of saccharides, are subject to slight shifts of wavenumbers indicating a hydrogen bonding reorganization (Stuart, 2004). Also, the region below 900 cm^{-1} occurs changed indicating the contribute of the typical vibrational mode of Chl*a*-pyrrol ring (Mandal et al., 2015). Amide I and amine signals (region 1500–1800 cm^{-1}, Fig. 4a) present again an intensity inverted ratio. All these changes can be interpreted, in agreement with showed UV–Vis absorption spectroscopy results, considering that Chl*a* interacts with CH/CD rearranging the polymer chains association specifically involving the chitosan-amino groups. In accordance with several observations reported in literature (Cellamare et al., 2013; Mandal et al., 2015; Omata & Murata, 1980), it is possible to assume a coordination between the cationic NH_3^+ group presents on the CH chain and Chl*a* macrocycle (Mandal et al., 2015). In order to confirm these hypotheses arising from spectroscopic and calorimetric techniques additional information were searched for through Water Vapor Transmission Rate investigation.

3.5. Water Vapor Transmission Rate (WVTR)

WVTR of CH-based composite films with 2-HP-β-CD and Chl*a* are reported in Fig. S2. The effect due to the standard procedure modification necessary to prepare CH films has been also evaluated. As expected the incorporation of different molecules from chitosan, and the modification of the procedure to prepare CH films induces changes on the WVTR. Indeed by comparing results related to CH films and CH STD one, reported in Fig. S2, WVTR appears in the former to be around 800 g/m^2/day, in the latter around 550 g/m^2/day. Thus, the modification introduced by changing the film preparation procedure induces an increase of about 48% in the WVTR values. On the other hand, the addition of 2-HP-β-CD results in a WVTR decrease, *i.e.* around 250 g/m^2/day (about a decrease of 70% respect to CH film and 55% respect to CH standard films).

These results, as showed also by FTIR-ATR and DSC analysis, evidence a negative impact of film modification on the WVTR due to the presence of novel chitosan chains arrangement inside neutralized CH films if compared with CH STD one, allowing the transmission of water molecules (Philippova, Volkov, Sitnikova, & Khokhlov, 2001).

Always in accordance with FTIR-ATR analysis, the presence of 2-HP-β-CD induces the condensation of counterions on the charged groups of polymer chains, reducing the positive charge of macromolecules. The latter process induce the aggregation of chitosan chains (Xu, Kim, Hanna, & Nag, 2015). About this aspect, Demarger-Andre *and co*-workers (1994) show that the water content in CH films is related to the amount of NH_3^+ groups and their neutralization (from NH_3^+ in NH_2) makes the film less hygroscopic than those obtained as prepared (Chen et al., 2008). In our case, according to FTIR data, it seems that the acetate ion plays a similar role forming ion pairs with protonated amino groups of CH chains, thus affecting the hydrophobic character of CH films changing the WVTR through the films. This could be attributed (Xu et al., 2015) to the difficulty in acetate ion removal in presence of 2-HP-β-CD confirmed also by FTIR-ATR analysis. The same decrease in WVTR was observed after the treatment with EtOH (see Fig. S2) attributable to the dehydration effect of the organic molecule. In particular the hydrophilic CH chains interactions are removed in order to form a more stable ones with the elimination of water channels. For CH/CD films, the effect of EtOH treatment is a WVTR decreasing of 80% compacting CH structure by inducing novel H-

bonds arrangement and improving the intrinsic hydrophobic property of CH/CD films (Coates, 2000).

The introduction of Chl*a* in CH/CD films (Fig. S2) reduces even more the WVTR due to the hydrophobic character of Chl*a* that prevents water molecule diffusing through the film and to the coordination of protonated amino groups by the pigment (Coates, 2000). Both these effects induce the formation of hydrophobic interactions. These results were in accordance with XPS, DSC and FTIR data in which the Chl*a* presence induces arrangement on chitosan chains in which the NH_3^+ groups are involved.

3.6. SEM analysis

SEM images reported in Fig. S3 show that the CH films prepared with the standard (Fig. S3a) and the new procedure (Fig. S3b) have a similar morphology, *i.e.*, the films are homogeneous and smooth, however they present some protruding nodules. The same results have been obtained for CH/CD film (data not shown). The overall morphology of the CH film prepared with the new method and also with the standard one (data not shown) does not change significantly after immersion in ethanol (Fig. S3c), however, it is worth mentioning that EtOH immersion seems to slightly increase the surface roughness of the films, as also observed by AFM (see Section 3.7). The nodules present in the CH films (Fig. S3, panels b and c) disappear in the CH/CD film immersed in ethanol (Fig. S3d); indeed in the latter case the formation of some depressions is observed (arrows in Fig. 2d). Depressions seem uniformly distributed over the entire surface of the sample. This evidence suggests that the incorporation of 2-HP-β-CD induces changes in the arrangement and packing of CH polymer chains and, therefore in accordance with our discussion, alters the surface morphology of the film. The morphology of the CH/CD film does not change significantly when Chl*a* is present (Fig. S3e); while the homogeneity of the CH/CD/Chl*a* film indicates that a quite uniform distribution of Chl*a* is obtained in the layer. Results were in accordance with the clear homogenous distribution of the pigment inside the film (see picture in Fig. 1).

3.7. AFM analysis

In order to present a deepest morphological investigation, the analysis of, "as prepared" and upon EtOH treatment, CH STD, CH as well as CH/CD films has been carried out by means of AFM images, reported in Fig. 5. Even though the films of CH STD (Fig. 5a) and CH (Fig. 5b) show a homogeneous distribution, according to SEM analysis, the CH film appears more rough ($R_q = 1.5$ nm) than the CH STD ($R_q = 0.5$ nm). Such experimental evidence could be ascribed to the large amount of CH in the latter one. In particular, the hydrogen bonds are believed to play an essential role in organizing the macromolecules of CH chains (Philippova et al., 2001). In accordance with previous showed data, the chains organization is essentially due to intra- and intermolecular interactions in the case of CH STD film (Philippova et al., 2001).

On the other hand, we suppose that at lower amount of CH chains than in CH STD, like in the case of CH film, the intramolecular interactions are present in a preponderant way, so that it shows a structure less dense compared to that one of CH STD, in which we suppose the presence of inter-domains water channels.

The introduction of CD makes more smooth the CH film, so that the R_q value decreases to 1.1 nm (Fig. 5c). Likely further hydrogen bonds (Burns et al., 2015) between molecules make to rearrange the CH chains differently in a closely packed fashion. Such experimental evidence, strengthens FTIR data showing that the interactions in CH/CD films are quite similar to CH STD ones thus suggesting that H − bonds are responsible of the interactions between CH and 2-HP-β-CD (Burns et al., 2015). Such a hypothesis is further confirmed in the corresponding AFM phase images. Indeed, it is clearly evident that the introduction of CD (Fig. S4b) changes notably the organization of CH film (Fig. S4a) thanks to the increasing interactions between the two different materials.

For the sake of comparison of CH film with ones obtained in the presence of Chl*a*, the effect of EtOH solution on CH morphology has been also evaluated. Upon treatment, by immersing such films in EtOH, AFM topographies were recorded and showed in Fig. 5d–e. First of all, an important modification in the structure of such films is observed with respect to the "as prepared" films (Fig. 5a–c). It is well known that CH is insoluble in EtOH, so that a reorganization of CH chains is supposed in a favorable thermodynamic situation, in "polystyene" fashion, as reported in literature (Coates, 2000) obviously due to the decrease of the polarity of medium. Moreover, while the R_q value for the CH STD film is retained, in the CH and CH/CD films treated with EtOH it is increased with respect to corresponding films before the treatment. However, the trend of R_q values of CH STD, CH and CH/CD is unchanged in both cases, with or without treatment with EtOH.

The AFM phase images of the CH (Fig. S4c) and CH/CD (Fig. S4d) films after immersing in EtOH highlight the presence, in the latter case, of a second material represented by 2-HP-β-CD thanks to different color contrast of spots with respect to background of image. It is clearly evident the "nanoparticle-dominant" structure of CH film treated with EtOH as proposed by Qing He and coworkers (Coates, 2000). In accordance with WVTR and FTIR-ATR data, CH films compact their structure in contact with EtOH inducing the formation of novel H-bonds. The effect is less pronounced in CH STD since the dehydrate compact structure is poor in water channel. Upon the introduction of Chl*a* in the CH/CD film a slightly increase of the R_q to 1.2 nm has been observed (Fig. 6a). However, the film appears quite homogeneous thus suggesting that the different materials (CH, CD, Chl*a*) are distributed regularly in the film. Such experimental evidence is confirmed also by AFM phase image (Fig. 6b).

3.8. X-ray diffraction results

To inspect the crystalline/amorphous nature of the chitosan-based films, X-ray diffraction data have been collected on CH STD, CH, CH/CD and CH/CD/Chl*a*, since it was demonstrated in literature (Coates, 2000; Ogawa, Hirano, Miyanishi, Yui, & Watanabe, 1984; Xu et al., 2015) that the polymorphism and crystallinity as well as the amorphous state strongly depends on its preparation methods (Ogawa, Toshifume & Masaru, 1992).

X-ray patterns collected on both standard and modified chitosan (Fig. S5) films show the existence of an amorphous phase for all the investigated samples. With respect to the standard (Fig. S5a), the incorporation of 2-HP-β-CD (Fig. S4b) and Chl*a* (Figure S5c) as well as of EtOH (Fig. S5d) did not significantly affects the amorphous nature of the films based on the modified chitosan (CH).

3.9. Photoactivity studies

Photoactivity of the film containing Chl*a* was investigated by combining time-resolved and steady-state spectroscopic and photochemical techniques. The excited triplet state of Chl*a* is the key transient intermediate for the photosensitization of $^1O_2$ and its effective generation upon light excitation is thus crucial for the photodynamic action. Laser flash photolysis with nanosecond time-resolution is a powerful tool for obtaining spectroscopic and kinetic features of excited triplets of porphyrinoid systems since these transient species exhibit intense absorptions in the visible region and possess lifetimes falling in the microsecond time regime (Ogawa et al., 1992). Fig. 7 shows the transient absorption spectrum

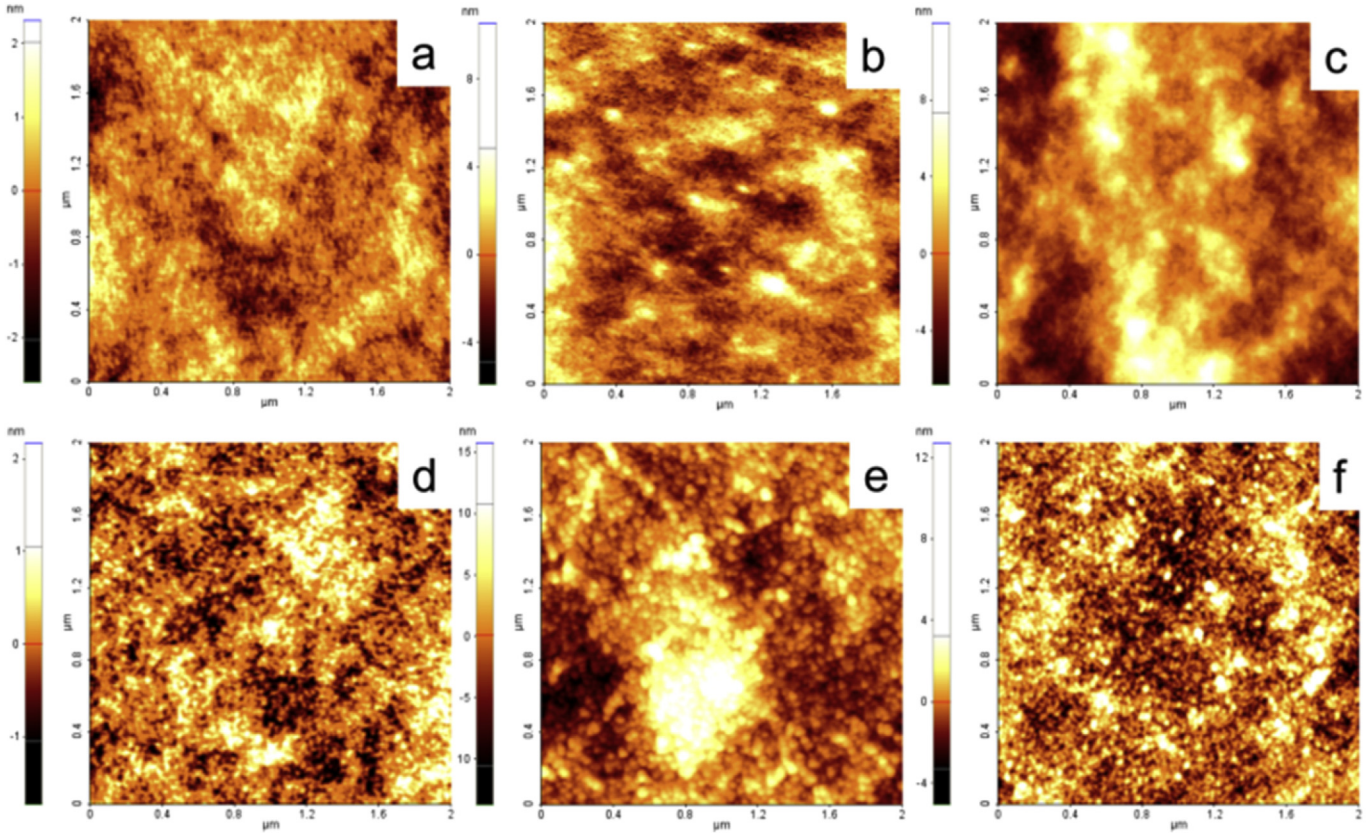

Fig. 5. AFM images of "as prepared" (a–c) and upon treatment with EtOH (d–f) related to CH STD, CH, and CH/CD films, respectively.

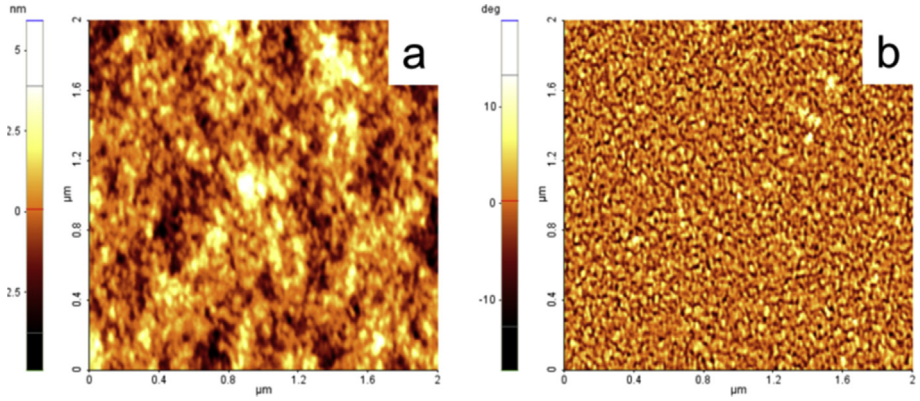

Fig. 6. AFM (a) topography and (b) phase of CH/CD/Chl a film.

recorded 0.2 μs after 355 nm laser excitation of the chitosan film containing Chl*a*. This transient spectrum shows the typical features of the excited triplet state of the Chl*a* with a maximum at ca. 460 nm and a bleaching due to the Soret ground-state absorption at ca. 410 nm. The triplet state decays mono-exponentially with a triplet lifetime of ca. 20 μs (inset Fig. 7). Furthermore, the time evolution of the absorbance changes reveals that no new transient species is formed concurrently to the triplet decay.

Energy transfer from the triplet of Chl*a* embedded in the chitosan film to molecular oxygen results in the concomitant photogeneration of $^1O_2$. Near-infrared luminescence spectroscopy is the most suitable technique to unequivocally demonstrate the generation $^1O_2$. This species, in fact, exhibits a typical phosphorescence signal at 1270 μm (He et al., 2011). In a typical experiment for $^1O_2$ detection, the film was placed in a spectrofluorimetric cuvettes containing 3 mL of D_2O, and excited with a CW laser at 405 nm D_2O was used as a solvent for $^1O_2$ luminescence measurements to take advantage of the larger radiative constant and longer lifetime with respect to H_2O. Fig. 8 shows clear-cut evidences for the $^1O_2$ photogeneration from film as proven by the characteristic luminescence spectrum in the NIR region, as result of the energy transfer from the lowest excited triplet state of the porphyrin to molecular oxygen.

In order to demonstrate that the photogenerated $^1O_2$ can diffuse out from the film and, consequently, able to react with substrates present in solution we carried out steady-state photolysis

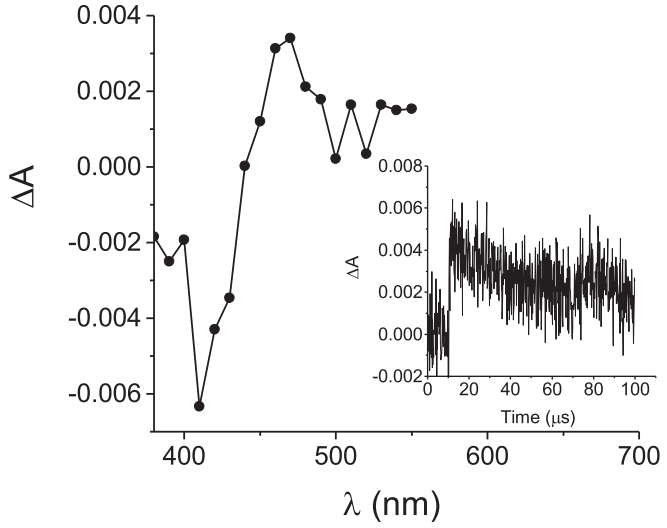

Fig. 7. Transient absorption spectrum observed 0.2 μs after 355 laser excitation of the CH/CD/Chla film. $E_{355} \approx 10$ mJ/pulse. The inset shows the decay profile monitored at 460 nm.

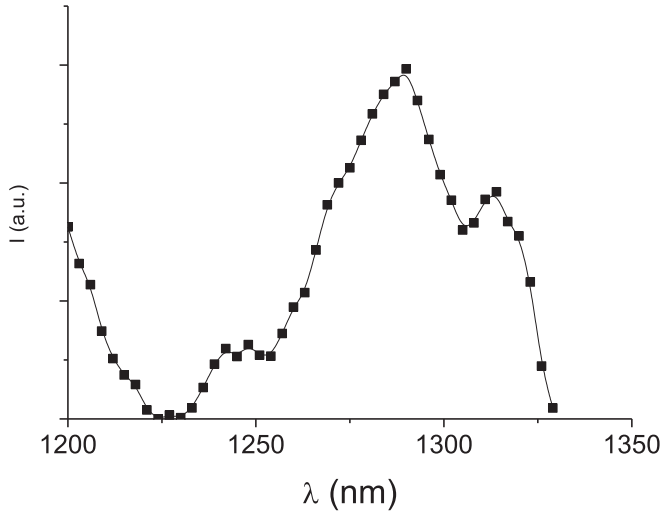

Fig. 8. Singlet oxygen luminescence observed upon 405 nm CW laser excitation (2 W cm^{-2}) of a CH/CD/Chla film immersed in D_2O.

experiments in the presence of S^4TdR (4-Thiotymidine) and SOSG (Singlet Oxygen Sensor Green) as suitable primary $^1O_2$ acceptors (Cellamare et al., 2013; Rizzi et al., 2014a; Rizzi et al., 2015; Ragas, Jimenez-Banzo, Sanchez-Garcia, Batllori & Nonell, 2009).

Fig. 9a,b shows results obtained upon irradiation of the film in the presence of SOSG and S^4TdR, respectively. The irradiation of the CH/CD/Chl*a* film immersed in a D_2O solution containing 10^{-5} M of S^4TdR, leads to the degradation of the latter (Fig. 9b), as evidenced by the bleaching of the main S^4TdR absorption band. Additionally, a red shift of the S^4TdR main absorption band from 326 nm to 337 nm was observed. This result is not surprising since it depends on the slight and slow releasing of H^+ from chitosan film, in such condition. In fact the absorption of S^4TdR at neutral and acid pH is settled at around 337 nm (Rizzi et al., 2014a; Montalti, Credi, Prodi & Gandolfi, 2006) as it is clear from UV–Vis absorption spectrum in H_2O (dashed line in Fig. 9b). In the inset of the same Figure, measurement of control in absence of Chl*a* is reported. In absence of photosensitizer, a clear red shifts of S^4TdR absorption peak is

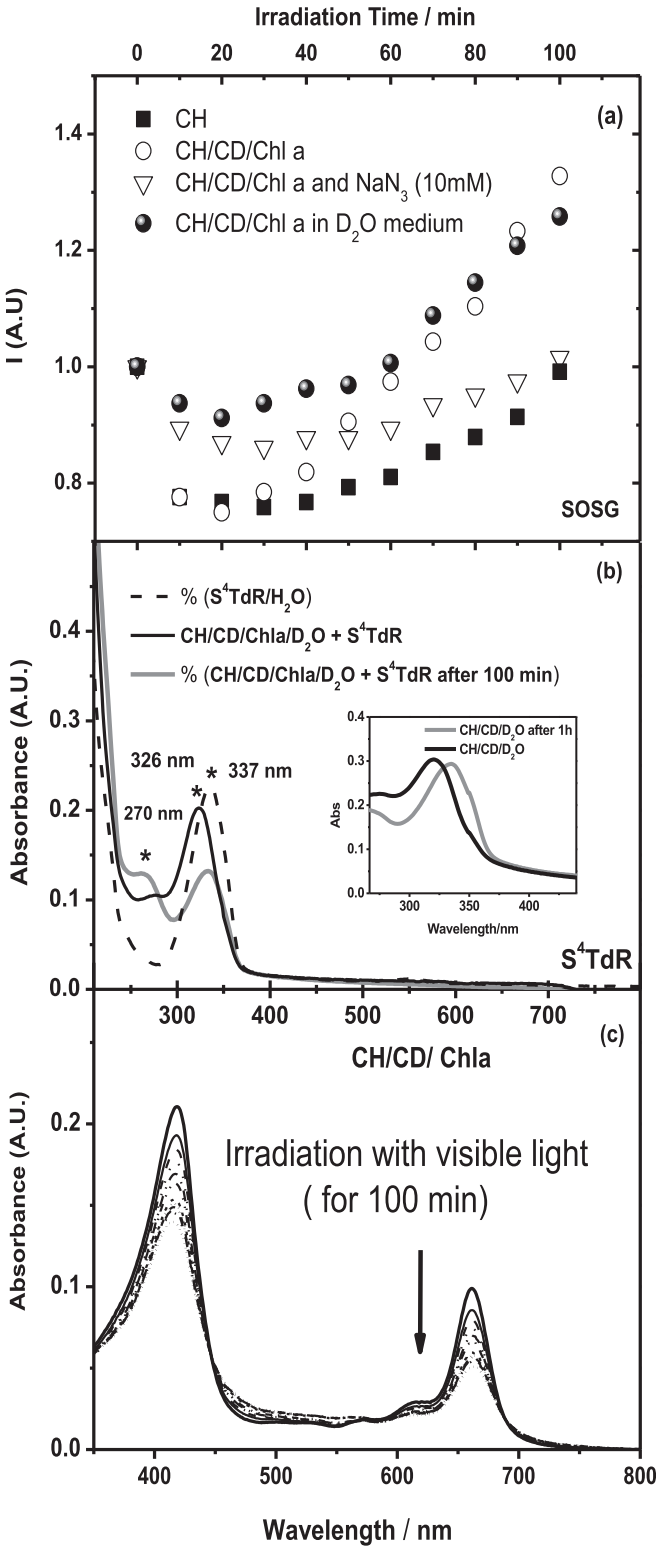

Fig. 9. (a)Time evolution of normalized fluorescence emission at 525 nm of SOSG 1.5 μM of aqueous solutions containing CH/CD/Chla film in different conditions. (see text for details). (b) Time evolution of S^4TdR absorption (10^{-5} M) spectrum of aqueous solutions containing CH/CD/Chla film. Dotted line was referred to an aqueous solution, pH 6.5, in absence of CH containing only S^4TdR (see text for details) (c) Time evolution of absorption CH/CD/Chla spectrum (see text for details) under visible.

showed after light irradiation, while it is not evidenced any absorbance decrease. Moreover as indicated in Fig. 9b, a new band

was detected at 270 nm when Chl*a* was presented in the composite film, indicating the conversion of S^4TdR in Thymidine as the main $^1O_2$-induced product (Rizzi et al, 2014a). Results obtained in the presence of SOSG (Fig. 9a), a selective $^1O_2$ probe, confirmed the previous consideration indicating the photoactivity of Chitosan/Chl*a* film under our experimental conditions.

In Fig. 9a are reported photolysis experiments performed both in aqueous solution and in D_2O medium, containing SOSG with CH/CD film and CH/CD/Chl*a* film in presence and in absence of NaN_3 (10 mM), a well-known $^1O_2$ quencher (Cellamare et al., 2013). Looking at Fig. 9a, a fluorescence intensity decrease was observed in the first time of reaction in all reported traces, with a subsequent fluorescence increase increasing the irradiation time. However, in D_2O medium, the initial fluorescence decrease appears reduced. As reported in a previous study performed by some of Authors of this paper (Cellamare et al., 2013), related to Chl*a* in water solutions, the initial fluorescence decrease is similar to the results obtained for SOSG without PS and irradiated in visible region. In fact, a fast intramolecular electron transfer from anthracene moiety to fluorescein moiety occurs quenching the SOSG fluorescence (Wilkinson, Helman & Ross, 1993; Ragas et al., 2009). Interestingly, this intramolecular electron transfer reaction competes efficiently with SOSG fluorescence if the anthracene moiety is not destroyed by singlet oxygen. As a consequence, when$^1O_2$ oxides the anthracene moiety to the endoperoxide product, the intra-electron transfer reaction does not occurs and the SOSG fluorescence increases. Not surprisingly, in the D_2O medium, where the $^1O_2$ lifetime occurs to be greater than the one observed in water solutions (Xu et al., 2015), a higher amount of anthracene moiety is oxidized by $^1O_2$ and subtracted from the intramolecular electron transfer reaction increasing the fluorescence intensity in the first part of reaction. Moreover, the comparison of the maximum fluorescence intensity values (see Fig. 9a), obtained in the different conditions, provides further information about the production of $^1O_2$ by chitosan film containing Chl*a*. In fact experiments in presence of NaN_3 confirm clearly the proposed hypothesis. A significant decrease of fluorescence intensity is observed comparing the I_{max} values recorded for CH/CD/Chl*a* film in either H_2O or D_2O without NaN_3. On the other hand, as shown in Fig. 9c, there is a progressive bleaching of Chl*a* absorbance with elapsing the irradiation time. In 10 min, the absorbance of main absorption bands in the red and blue regions decreases of about 15%. After a prolonged time of irradiation, the absorption intensity at 661 nm decreased of about 50% in 100 min, while an increase in absorbance intensity at wavelengths above 690 nm and between 460 and 580 nm was also observed. These results are in good agreement with those reported in literature (Barazzouk et al., 2012b). Barazzouk and co-workers (2012b) display studies in which the photodegradation of Chl*a* in several conditions was well described, ascribing such behavior to the production of ROS. Clearly the observed photobleaching of the pigment, under this condition, suggests that Chl*a* itself appears as an indirect molecular probe for toxic species, decreasing its absorption intensity during light irradiation.

The overall results indicate the involvement of $^1O_2$ and probably of other ROS. Procedures addressed to improve the photostabilty of Chl*a* preventing the ROS-attack will be developed, in the next future in our laboratories.

4. Conclusions

In the present paper, different Chitosan and Chitosan/2-HP-β-CD composite films have been obtained and the latter has been successfully modified by inserting Chl*a* casted by an ethanolic solution. An innovative procedure, recently developed in our laboratory has been employed to reduce the intrinsic acidity of chitosan film in order to introduce Chl*a* maintaining its physical and chemical properties. Each polysaccharide component of the composite films plays a specific role in the interactions with chitosan water-retained, and 2-HP-β-CD increasing the hydrophobic properties of the films. DSC and WVTR analyses show the increased hydrophobic character of the Chitosan films in the presence of 2-HP-β-CD and Chl*a* offering good perspective for extending shelf-life or improve safety properties maintaining the quality of the food. Our comprehensive investigation demonstrates that Chl*a* molecules have a strong affinity towards the Chitosan/2-HP-β-CD mixture and spectroscopic analyses indicate that Chl*a* interacts with amino groups of chitosan chains. The morphological investigations carried out by SEM and AFM images, demonstrate that Chl*a* is uniformly distributed on Chitosan film. In addition the contact with EtOH induces a novel chitosan chain interactions rendering the chitosan film structure much more compact than previous the treatment. XRD analysis shows the existence of an amorphous phase for all the investigated samples. Additionally the photodynamic effects of Chl*a* has been also investigated. Nanosecond laser flash photolysis technique provides clear evidence for the population of the excited triplet state of Chl*a* and the photogeneration of singlet oxygen is demonstrated by both direct detection by using infrared luminescence spectroscopy and chemical methods based on the use of suitable traps.

Acknowledgment

This study was supported by the PRIN-MIUR 2010–2011 (Prot. 2010C4R8M8) funding program: “Architetture ibride multifunzionali basate su biomolecole per applicazioni nel campo della sensoristica, della conversione di energia e del biomedicale”. We gratefully acknowledge the skilfull and excellent technical assistance of Mr. Sergio Nuzzo and Mr. Savino Cosmai and Dr. Andrea Ventrella for the excellent and precious collaboration in the determination of the chitosan acetylation degree.

Appendix A. Supplementary data

Supplementary data related to this article can be found at http://dx.doi.org/10.1016/j.foodhyd.2016.02.012.

References

Agostiano, A., Catucci, L., Castagnolo, M., Colangelo, D., Cosma, P., Fini, P., et al. (2002a). Interaction between chlorophyll a and beta-cyclodextrin derivatives in aqueous solutions - spectroscopic and calorimetric study. *Journal of Thermal Analysis and Calorimetry, 70*, 115–122.

Agostiano, A., Catucci, L., Colafemmina, G., & Della Monica, M. (1996). Chlorophyll a self-organization in microheterogeneous surfactant systems. *Biophysical Chemistry, 60*(1–2), 17–27.

Agostiano, A., Catucci, L., Colafemmina, G., & Scheer, H. (2002b). Role of functional groups and surfactant charge in regulating chlorophyll aggregation in micellar solutions. *The Journal of Physical Chemistry B, 106*, 1446–1454.

Agostiano, A., Catucci, L., Cosma, P., & Fini, P. (2003). Aggregation processes and photophysical properties of chlorophyll a in aqueous solutions modulated by the presence of cyclodextrins. *Physical Chemistry Chemical Physics, 5*, 2122–2128.

Agostiano, A., Cosma, P., & Della Monica, M. (1991). Formation of chlorophyll-a photoreactive dimers in alcoholic mixtures - spectroscopic and electrochemical study. *Journal of Photochemistry Photobiology A: Chemistry, 58*(2), 201–213.

Agostiano, A., Cosma, P., Della Monica, M., & Fong, F. K. (1990). Spectroscopic and electrochemical characterization of chlorophyll-a in different water + organic-solvent mixtures. *Bioelectrochemistry and Bioenergetics, 23*(3), 311–324.

Agostiano, A., Cosma, P., Trotta, M., Monsù-Scolaro, L., & Micali, N. (2002). Chlorophyll a behavior in aqueous solvents: formation of nanoscale self-assembled complexes. *The Journal of Physical Chemistry B, 106*(49), 12820–12829.

Baxter, A., Dillon, M., Taylor, K. D., & Roberts, G. A. F. (1992). Improved method for IR determination of the degree of N-acetylation of chitosan. *International Journal of Biological Macromolecules, 14*, 166–169.

Beamson, G., & Briggs, D. (1992). *High resolution XPS of organic polymers*. Chichester:

J. Wiley & Sons.
Bekalé, L., Barazzouk, S., & Hotchandani, S. (2012a). Beneficial role of gold nanoparticles as photoprotector of magnesium tetraphenylporphyrin. *Journal of Materials Chemistry, 22*, 2943–2951.
Bekalé, L., Barazzouk, S., & Hotchandani, S. (2012b). Enhanced photostability of chlorophyll-a using gold nanoparticles as an efficient photoprotector. *Journal of Matererials Chemistry, 22*, 25316–25324.
Belalia, R., Grelier, S., Benaissa, M., & Coma, V. (2008). New bioactive biomaterials based on quaternized chitosan. *Journal of Agricultural and Food Chemistry, 56*, 1582–1588.
Bordenave, N., Grelier, S., & Coma, V. (2010). Hydrophobization and antimicrobial activity of chitosan and paper-based packaging material. *Biomacromolecules, 11*, 88–96.
Bordenave, N., Grelier, S., Pichavant, F., & Coma, V. (2005). Water and moisture susceptibility of chitosan and paper-based materials: structure-property relationships. *Journal of Agricultural and Food Chemistry, 55*, 9479–9488.
Bostan, M. S., Mutlu, E. C., Kazak, H., Keskin, S. S., Oner, E. T., & Eroglu, M. S. (2014). Comprehensive characterization of chitosan/PEO/levan ternary blend films. *Carbohydrate Polymers, 102*, 993–1000.
Brace, J. G., Fong, F. K., Karweik, D. H., Koester, V. J., Shepard, A., & Winograd, N. (1978). Stoichiometric determination of chlorophyll a-water aggregates and photosynthesis. Symbiotic roles of the magnesium atom and the ring V cyclopentanone group in the structural and photochemical properties of chlorophyll a monohydrate and dehydrate. *Journal of the American Chemistry Society, 100*, 5203-2507.
Burns, N. A., Burroughs, M. C., Gracz, H., Pritchard, C. Q., Brozena, A. H., Willoughby, J., et al. (2015). Cyclodextrin facilitated electrospun chitosan nanofibers. *RSC Advances, 5*, 7131–7137.
Cellamare, B. M., Fini, P., Agostiano, A., Sortino, S., & Cosma, P. (2013). Identification of ROS produced by photodynamic activity of Chlorophyll/Cyclodextrin inclusion complexes. *Photochemistry and Photobiology, 89*, 432–441.
Cerveny, K. E., De Paola, A., Duckworth, S. H., & Gulig, P. A. (2002). Phage therapy of local and systemic disease caused by Vibrio vulnificus in iron-dextran-treated mice. *Infection and Immunity, 70*, 6251–6262.
Chauvet, J. P., Viovy, R., Santus, R., & Land, E. J. (1981). One-electron oxidation of photosynthetic pigments in micelles. Bacteriochlorophyll a, chlorophyll a, chlorophyll b, and pheophytin a. *The Journal of Physical Chemistry, 85*(23), 3449–3456.
Chen, P. H., Kuo, T. Y., Liu, F. H., Hwang, Y. H., Ho, M. H., Wang, D. M., et al. (2008). Use of dicarboxylic acids to improve and diversify the material properties of porous chitosan membranes. *Journal of Agricultural and Food Chemistry, 56*, 9015–9021.
Chen, G., Mi, J., Wu, X., Luo, C. L., Li, J. B., Tanng, Y. X., et al. (2011). Structural features and bioactivities of the chitosan. *International Journal of Biological Macromolecules, 49*, 543–547.
Coates, J. (2000). Interpretation of infrared spectra, a practical approach. In R. A. Meyers (Ed.), *Encyclopedia of analytical chem* (pp. 10815–10837). Chichester: John Wiley & Sons Ltd.
Coma, V. (2013). Polysaccharide-based biomaterials with antimicrobial and antioxidant properties. *Polímeros, 23*(3), 287–297.
Davies, D. H., Elson, C. M., & Hayes, E. R. (1989). *Chitin and chitosan: sources, chemistry, biochemistry, physical properties and applications*. In G. Skjak-Braek, T. Anthonsen, & P. Sandford (Eds.) (pp. 467–472). England: Elsevier Appl. Sci.
Demarger-Andre, S., & Domard, A. (1994). Chitosan carboxylic acid salts in solution and in the solid state. *Carbohydrate Polymers, 23*, 211–219.
Dentuto, P. L., Catucci, L., Cosma, P., Fini, P., Agostiano, A., Hackbarth, S., et al. (2007). Cyclodextrin/chlorophyll a complexes as supramolecular photosensitizers. *Bioelectrochemistry, 70*, 39–43.
El Ghaouth, A., Arul, J., Grenier, J., & Asselin, A. (1992). Antifungal activity of chitosan on 2 postharvest pathogens of strawberry fruits. *Phytopathology, 82*, 398–402.
El Ghaouth, A., Arul, J., Ponnampalam, R., & Boulet, M. (1991). Chitosan coating effect on storability and quality of fresh strawberries. *Journal of Food Science, 56*, 1618–1620.
El-Hefian, E. A., Nasef, M. M., & Yahaya, A. H. (2012). Preparation and characterization of chitosan/Agar blended films: Part 1. Chemical structure and morphology. *E-Journal of Chemistry, 9*(3), 1431–1439.
Fu, D., Jordan, J. J., & Samson, L. D. (2013). Human ALKBH7 is required for alkylation and oxidation-induced programmed necrosis. *Genes & Development, 27*, 1089–1100.
Gomez-Estaca, J., Lopez-de-Dicastillo, C., Hernandez-Munoz, P., Catala, R., & Gavara, R. (2014). Advances in antioxidant active food packaging. *Trends in Food Science & Technology, 35*, 42–51.
Hamblin, M. R., & Hasan, T. (2004). Photodynamic therapy: a new antimicrobial approach to infectious disease? *Photochemical and Photobiological Sciences, 3*(5), 436–450.
Harish Prashanth, K. V., Kittur, F. S., & Tharanathan, R. N. (2002). Solid state structure of chitosan prepared under different N-deacetylating conditions. *Carbohydrate Polymers, 50*(1), 27–33.
He, Q., Ao, Q., Gong, Y., & Zhang, X. (2011). Preparation of chitosan films using different neutralizing solutions to improve endothelial cell compatibility. *Journal of Materials Science: Materials in Medicine, 22*, 2791–2802.
Jiang, Y., & Li, Y. (2001). Effects of chitosan coating on postharvest life and quality of longan fruit. *Food Chemistry, 73*, 139–143.
Jug, M., Maestrelli, F., & Mura, P. (2012). Native and polymeric β-cyclodextrins in performance improvement of chitosan films aimed for buccal delivery of poorly soluble drugs. *Journal of Inclusion Phenomena Macrocyclic Chemistry, 74*, 87–97.
Kang, J., Liu, H., Zheng, Y.-M., Qu, J., & Chen, J. (2010). P.Systematic study of synergistic and antagonistic effects on adsorption of tetracycline and copper onto a chitosan. *Journal of Colloid and Interface Science, 344*, 117–125.
Karweik, D. H., & Winograd, N. (1976). Nitrogen charge distributions in free-base porphyrins, metalloporphyrins, and their reduced analogs observed by X-ray photoelectron spectroscopy. *Inorgonic Chemistry, 15*, 2336–2342.
Kasaai, R. (2008). A review of several reported procedures to determine the degree of N-acetylation for chitin and chitosan using infrared spectroscopy. *Carbohydrate Polymers, 71*, 497–508.
Kittur, F. S., Harish Prashanth, K. V., Sankar, K. U., & Tharanathan, R. N. (2002). Characterization of chitin, chitosan and their carboxymethyl derivatives by differential scanning calorimetry. *Carbohydrate Polymers, 49*(2), 185–193.
Krajewska, B. (1991). Chitin and its derivatives as supports for immobilization of enzymes. *Acta Biotechnologica, 11*, 269–277.
Krajewska, B., Leszko, M., & Zaborska, W. (1990). Urease immobilized on chitosan membrane - preparation and properties. *Journal of Chemical Technology and Biotechnology, 48*, 337–350.
Krouit, M., Granet, R., Branland, P., Verneuil, B., & Krausz, P. (2006). New photoantimicrobial films composed of porphyrinated lipophilic cellulose esters. *Bioorganic & Medicinal Chemistry Letters, 16*(6), 1651–1655.
Krouit, M., Granet, R., & Krausz, P. (2009). Photobactericidal films from porphyrins grafted to alkylated cellulose – synthesis and bactericidal properties. *European Polymer Journal, 45*(4), 1250–1259.
Lavertu, M., Xia, Z., Serreqi, A. N., Berrada, M., Rodrigues, A., Wang, D., et al. (2003). Validated 1H NMR method for the determination of then degree of deacetylation of chitosan. *Journal of Pharmaceutical and Biomedical Analysis, 32*, 1149–1158.
Liu, H., Adhikari, R., Guo, Q., & Adhikari, B. (2013). Preparation and characterization of glycerol plasticized (high-amylose) starch–chitosan films. *Journal of Food Engineering, 116*, 588–597.
Mandal, P., Manna, J. S., Das, D., & Mitra, M. K. (2015). Excitonic dynamics of Chlorophyll-a molecules in chitosan hydrogel scaffold. *Journal of Photochemical and Photobiological Sciences, 14*, 786–791.
Manna, J. S., Basu, S., Mitra, M. K., Mukherjee, S., & Das, G. C. (2009). Study on the biostability of chlorophyll a entrapped in silica gel nanomatrix. *Journal of Materials Science: Materials in Electronics, 20*, 1068–1072.
Mbakidi, J. P., Herke, K., Alvès, S., Chaleix, V., Granet, R., Krausz, P., et al. (2013). Synthesis and photobiocidal properties of cationic porphyrin-grafted paper. *Carbohydrate Polymers, 91*(1,2), 333–338.
Moczek, L., & Nowakowska, M. (2007). Novel water-soluble photosensitizers from chitosan. *Biomacromol., 8*, 433–438.
Montalti, M., Credi, A., Prodi, L., & Gandolfi, M. T. (2006). *Handbook of photochemistry* (3rd ed.). BocaRaton: CRC Press.
Muzzarelli, R. A. A., & Rocchetti, R. (1986). In R. A. A. Muzzarelli, C. Jeuniaux, & G. W. Gooday (Eds.), *Chitin in nature and technology* (pp. 385–388). New York: Plenum Press.
Nunthanid, J., Puttipipatkhachorn, S., Yamamoto, K., & Peck, G. E. (2001). Physical properties and molecular behavior of chitosan films. *Drug Development and Industrial Pharmacy, 27*(2), 143–157.
Ogawa, K., Hirano, S., Miyanishi, T., Yui, T., & Watanabe, T. (1984). A new polymorph of chitosan. *Macromolecules, 17*, 973–975.
Ogawa, K., Toshifume, Y., & Masaru, M. (1992). Dependece on the preparation of the polymorphism and cristallinity of chitosan membranes. *Bioscience, Biotechnology, and Biochemistry, 56*(6), 858–862.
Omata, T., & Murata, N. A. (1980). A rapid and efficient method to prepare chlorophyll a and b from leaves. *Photochemistry and Photobiology, 31*, 183–185.
Pedersen, M. F., Stæhr, P. A., Wernberg, T., & Thomsen, M. S. (2005). Biomass dynamics of exotic Sargassum muticum and native Halidrys siliquosa in Limfjorden, Denmark – implications of species replacements on turnover rates. *Aquatic Botany, 83*, 31–47.
Pereira, V. A., Jr., Queiroz de Arruda, I. N., & Stefani, R. (2015). Active chitosan/PVA films with anthocyanins from Brassica oleraceae (red cabbage) as time–temperature indicators for application in intelligent food packaging. *Food Hydrocolloids, 43*(1), 180–188.
Philippova, O. E., Volkov, E. V., Sitnikova, N. L., & Khokhlov, A. R. (2001). Two types of hydrophobic aggregates in aqueous solutions of chitosan and its hydrophobic derivative. *Biomacromolecules, 2*, 483–490.
Quintavalla, S., & Vicini, L. (2002). Antimicrobial food packaging in meat industry. *Meat Science Industry, 62*(3), 373–380.
Rabea, E. I., Badawy, M. E. T., Stevens, C. V., Smagghe, G., & Steurbaut, W. (2003). Chitosan as antimicrobial agent: applications and mode of action. *Biomacromolecules, 4*, 1457–1465.
Ragas, X., Jimenez-Banzo, A., Sanchez-Garcia, D., Batllori, X., & Nonell, S. (2009). Singlet oxygen photosensitisation by the fluorescent probe singlet oxygen sensor green. *Chemical Communications, 20*, 2920–2922.
Ringot, C., Sol, V., Barrière, M., Saad, N., Bressollier, P., Granet, R., et al. (2011). Triazinyl porphyrin-based photoactive cotton fabrics: preparation, characterization, and antibacterial activity. *Biomacromolecules, 12*(5), 1716–1723.
Rizzi, V., Losito, I., Ventrella, A., Fini, P., Agostiano, A., Longobardi, F., et al. (2014a). pH-related features and photostability of 4-thiothymidine in aqueous solution: an investigation by UV-visible, NMR and FTIR-ATR spectroscopies and by electrospray ionization mass spectrometry. *RSC Advances, 4*, 48804–48814.
Rizzi, V., Longo, A., Fini, P., Semeraro, P., Cosma, P., Franco, E., et al. (2014b). Applicative study (part I): the excellent conditions to remove in batch direct

textile dyes (direct red, direct blue and direct yellow) from aqueous solutions by adsorption processes on low-cost chitosan films under different conditions. *Advances in Chemical Engineering and Science, 4*, 454–469.

Rizzi, V., Losito, I., Ventrella, A., Fini, P., Fraix, A., Sortino, S., et al. (2015). Rose Bengal-photosensitized oxidation of 4-thiothymidine in aqueous medium: evidence for the reaction of the nucleoside with singlet state Oxygen. *Physical Chemistry Chemical Physics, 17*, 26307.

Roy, P. S., Samanta, A., Mukherjee, M., Roy, B., & Mukherjee, A. (2013). Designing novel pH-induced chitosan–gum odina complex coacervates for colon targeting. *Industrial & Engineering Chemistry Research, 52*, 15728–15745.

Ryan, A. A., & Senge, M. O. (2015). How green is green chemistry? Chlorophylls as a bioresource from biorefineries and their commercial potential in medicine and photovoltaics. *Photochemistry Photobiological Sciences, 14*, 638–660.

Sajjan, U. S., Tran, L. T., Sole, N., Rovaldi, C., Akiyama, A., Friden, P. M., et al. (2001). P-113D, an antimicrobial peptide active against Pseudomonas aeruginosa, retains activity in the presence of sputum from cystic fibrosis patients. *Antimicrobial Agents and Chemotherapy, 45*, 3437–3444.

Shrestha, A., & Kishen, A. (2012). Polycationic chitosan-conjugated photosensitizer for antibacterial photodynamic therapy. *Photochemistry and Photobiology, 88*, 577–583.

Stuart, B. H. (2004). Infrared spectroscopy: fundamentals and applications. In *Analytical technique in the sciences*. Wiley.

Synytsya, A., Grafova, M., Slepicka, P., Gedeon, O., & Synytsya, A. (2012). Modification of chitosan–methylcellulose composite films with meso-Tetrakis(4-sulfonatophenyl)porphyrin. *Biomacromolecules, 13*(2), 489–498.

Thakhienw, W., Devahastin, S., & Soponronnarit, S. (2013). Physical and mechanical properties of chitosan films as affected by drying methods and addition of antimicrobial agent. *Journal of Food Engineering, 119*, 140–149.

Vermeiren, L., Devlieghere, F., Van Beest, M., De Kruijf, N., & Debevere, J. (1999). Developments in the active packaging of foods. *Trends in Food Science & Technology, 10*, 77–86.

Wainwright, M. (1998). Photodynamic antimicrobial chemotherapy (PACT). *Journal of Antimicrobial Chemotherapy, 42*(1), 13–28.

Wang, H. D., Chu, L. Y., Song, H., Yang, J. P., Xie, R., & Yang, M. (2007). Preparation and enantiomer separation characteristics of chitosan/β-cyclodextrin composite membranes. *Membrane Science, 297*, 262–270.

Wilkinson, F., Helman, W. P., & Ross, A. B. (1993). Quantum yield for the photosensitized formation of the lowest electronically excited state of molecular oxygen in solution. *Journal of Physical and Chemical Reference Data, 22*, 113–262.

Xu, Y. X., Kim, K. M., Hanna, M. A., & Nag, D. (2015). Chitosan–starch composite film: preparation and characterization. *Industrial Crops and Products, 21*, 185–192.

Yoshikawa, T. T. (2002). Antimicrobial resistance and aging. *Journal of the American Geriatrics Society, 50*, S226–S229.